Huyen, PT.; Trinh, VD.; Portilla, MT.; Martínez, C. (2021). Influence of boron promotion on the physico-chemical properties and catalytic behavior of Zn/ZSM-5 in the aromatization of n-hexane. Catalysis Today. 366:97-102. https://doi.org/10.1016/j.cattod.2020.03.030

Influence of boron promotion on the physico-chemical properties and catalytic behavior of Zn/ZSM-5 in the aromatization of n-hexane

Pham Thanh Huyen[1*], Vu Dinh Trinh[1], M. Teresa Portilla[2], Cristina Martínez[2*]

[1]*School of Chemical Engineering, Hanoi University of Science and Technology, Vietnam,*

[2] *Instituto de Tecnología Química, Universitat Politècnica de València – Consejo Superior de Investigaciones Científicas, Spain*

[*]*Corresponding authors: huyen.phamthanh@hust.edu.vn; cmsanche@itq.upv.es*

Abstract

The characterization and catalytic performance of Zn/ZSM-5 and Zn-B/ZSM-5 catalysts in the n-hexane aromatization was reported. Catalysts were prepared by post-synthesis impregnation and thoroughly characterized by means of XRD, Py-FTIR, N_2 adsorption, ^{27}Al and ^{11}B MAS NMR spectroscopy and electron microscopy techniques. The incorporation of zinc reduces the Brønsted acid site density and increases the Lewis acidic sites of the final ZSM-5 based catalysts. The presence of boron slightly reduces the initial activity of the catalyst but slows down its deactivation rate.

Keywords: Aromatization, Pyridin FTIR, Zn-modified ZSM-5 zeolite, Boron promoter.

1. Introduction

ZSM-5 zeolite is a microporous aluminosilicate material with well-defined pore structure and composition, which is widely used as acid catalyst in alkylation, acylation, isomerization, cracking and aromatization [1,2]. Converting low alkanes (C2 – C6) into

aromatic compounds is of great industrial interest, and a number of processes such as Cyclar (BP-UOP) [3,4], M-2 forming (Mobil) [5] and Aroforming (IFP/SALUTEC) [6] are commercially available. Many studies on the aromatization of light hydrocarbons show that ZSM-5 containing Zn or Ga are the most suitable for this kind of reaction [7-9]. The bifunctional catalyst provides metal sites for the dehydrogenation and hydrogenation, and acid sites for the oligomerization, isomerization and cyclization to convert light n-paraffins into BTX products. The medium pore structure of ZSM-5 favors aromatization into these BTX compounds and limits the formation of bulkier aromatics and coke precursors by shape selectivity. The introduction of Zn is known to increase the selectivity to aromatics by providing an alternative path via dehydrogenation of the alkane [10]. Moreover, the presence of Zn species results in significant changes of the acidic properites of ZSM-5, reducing the Brönsted acid site density proportionally to the Zn loading, and generating new relatively strong Lewis acid sites [11, 12].

The method employed for Zn incorporation into the ZSM-5 zeolite has an important effect on the acidic properties of the final catalysts and on the active species formed [13]. Thus, Zn introduction by means of ion exchange was shown to provided a higher fraction of surface $ZnOH^+$ species, responsible for alkane dehydrogenation as compared to other methods such as incipient wetness impregnation, physical mixture of the zeolite with ZnO or incorporation by direct synthesis, leading to the highest selectivity to aromatics in the conversion of methanol to aromatics.

Catalyst deactivation by coke deposition is an important problem in alkane aromatization processes. Boron promoted Ni-based catalysts were seen to be more resistant to deactivation by carbon deposition [14], but also more active for the decomposition of toluene (as model

compound for tar) [15]. J.B. Kimble et al. [16] claim the use of boron-promoted Zn/ZMS-5 as catalyst for the conversion of a low value naphtha stream into olefins and aromatics. B-Zn/ZSM-5 is more selective to the desired products and produces less coke. In this work, the effect of boron promotion on the physico-chemical properties and on the catalytic behavior of Zn/ZSM-5 in the aromatization of n-hexane has been studied.

2. Experimentals

2.1. Catalysts synthesis

Nano ZSM-5 zeolite with Si/Al ratio of 13 was supplied by Dalian Ligong Qiwangda Chemical Technology (Dalian, China) (http://en.dqtech.cn/). Zinc (5% wt.) was incorporated into these nano ZSM-5 by ion exchange of the zeolite with a 0.1M $Zn(NO_3)_2$ aqueous solution for 5 hours at 80°C under vigorous stirring, followed by filtration, washing, drying at 110°C for 3 hours and finally calcining at 520°C for 3 hours (heating rate of 1°C/min). Boric acid (0,094M) was used as the precursor for loading B (0.5% wt.) onto catalyst by suspending the Zn/ZSM-5 in the acid solution under vigorous stirring at 80°C for 5 hours, followed by filtration, drying at 110°C for 3 hours and finally calcining at 520°C (heating rate of 1°C/min) for 3 hours to obtain 5%Zn-0.5%B/ZSM-5 catalyst (Zn-B/ZSM-5).

2.2. Catalysts characterization

Powder X-Ray Diffraction (PXRD) measurements were performed with a PANalytical CUBIX diffractometer equipped with a PANalytica X'Celerator detector, operating at 45 kV and 40 mA, and using Cu Kα radiation (λ_1 = 0.15406 nm, λ_2 = 0.15444 nm, I_2/I_1=0.5),

N_2 adsorption/desorption isotherms were obtained at -195.3ºC using a TriStar 3000 MicroMeritics. Before adsorption measurements, the sample was degassed in nitrogen at 350ºC for 5 hours. FTIR was combined with pyridine adsorption–desorption. These measurements were done with a Nicolet 710 FTIR spectrometer on self-supported wafers (10 mg cm^{-1}) of samples previously activated at 400ºC and 10^{-2} Pa for 2 hours. After wafer activation, the base spectrum was recorded and pyridine vapor (6.5 x 10^2 Pa) was admitted in the vacuum IR cell and adsorbed onto the zeolite. Desorption of pyridine was performed under vacuum over three consecutive one-hour periods of heating at 150ºC, 250ºC and 350ºC, each of them followed by the IR measurement at room temperature. The spectra were scaled according to the sample weight. Chemical composition of the zeolites was determined, after their dissolution in a HNO_3/HCl/HF aqueous solution, in a Varian 715-ES ICP optical emission spectrometer. The morphology of the zeolites and dispersion of the metal was studied by field-emission scanning electron microscopy (FESEM) using a ZEISS Ultra-55 microscope, and by high-resolution transmission electron microscopy (HRTEM) using a JEM 2100F microscope.

2.3. Catalytic activity measurement

The catalytic activity tests were carried out in a glass fixed bed reactor loaded with 0.2g catalyst. The reactor temperature was increased to 400ºC and maintained at this temperature for 30 minutes under nitrogen flow (10 ml/min) to eliminate all moisture in the system and to activate the catalyst. After that, the temperature was adjusted to the desired reaction temperature, and n-hexane was added by saturation of a 10 ml/min nitrogen stream at 10ºC. The products were analyzed online by means of a Shimadzu GC 14B equipped with a FID detector. Samples were taken every of 30 minutes.

3. Results and Discussion

3.1. Catalysts characterization

The XRD patterns of the ZSM-5 zeolite samples Zn/ZSM-5 and Zn-B/ZSM-5 are compared in Fig. 1 with that of the parent ZSM-5.

All catalysts showed the characteristic powder XRD patterns of MFI topology with the main diffraction lines at 2θ = 7-10 and 20-25 [11, 17-19]. Addition of Zn and B onto the ZSM-5 zeolite does not affect the ZSM-5 structure, but the intensity of the main diffraction lines after Zn loading is slightly reduced. Considering 100% crystallinity for the parent ZSM-5, Zn/ZSM-5 and Zn-B/ZSM-5 have crystallinities of 88.5 and 88.0, respectively. Moreover, MFI belongs to the pentasil zeolites family and, under particular synthesis conditions, ZSM-5 can co-crystallize with the other pentasil zeolite ZSM-11 (MEL structure) leading to a disordered structure formed by the intergrowth of MFI and MEL [20-22]. The presence ZSM-11 is evidenced by the broadening –and disappearance at high MEL concentrations- of reflection (133) at ca. 24.4° 2θ. A careful inspection of the 22.5-25º 2θ region shows well defined diffraction lines, including the one corresponding to the (133) reflection, evidencing the absence of the MEL phase and confirming the zeolites as pure ZSM-5.

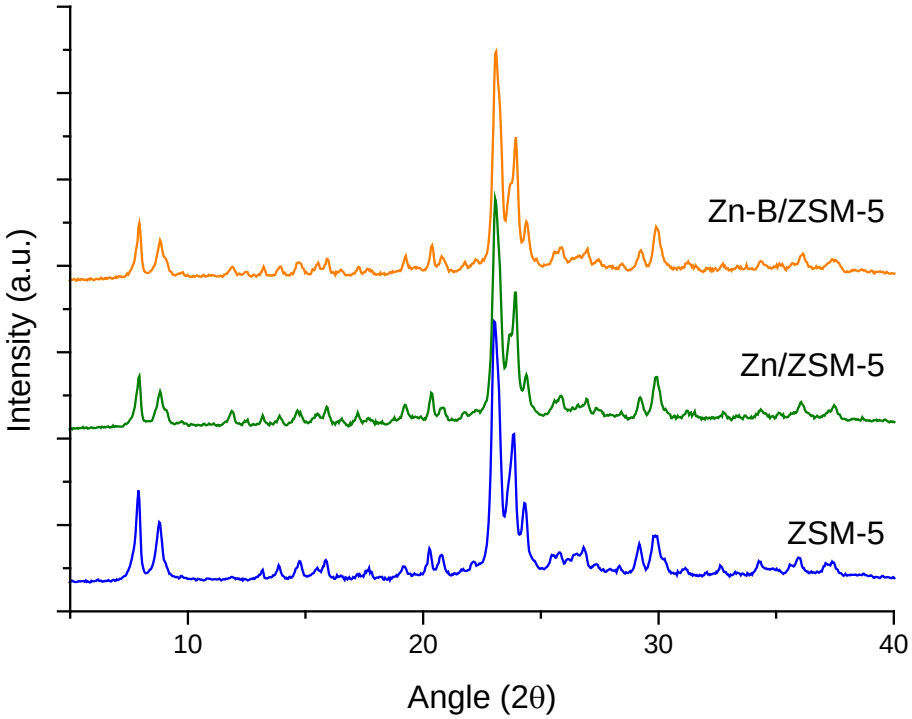

Fig. 1. XRD patterns of ZSM-5, Zn/ZSM-5 and Zn-B/ZSM-5.

Despite the high Zn loading (5.3 and 4.5% wt. as determined by ICP for the Zn/ZSM-5 and Zn-B/ZSM-5, respectively, see Table 1), no diffraction lines corresponding to Zn crystallites were observed in the Zn-zeolites, indicating that the metal species in the samples were highly dispersed [18].

The dispersion of the Zn species was further studied by electron microscopy. Fig. 2A shows the presence of small uniformly sized Zn particles, very well dispersed according to the FESEM images taken with a back-scatering detector. The average Zn particle size was estimated by HRTEM to be below 5 nm (see Fig. 2B).

A) B)

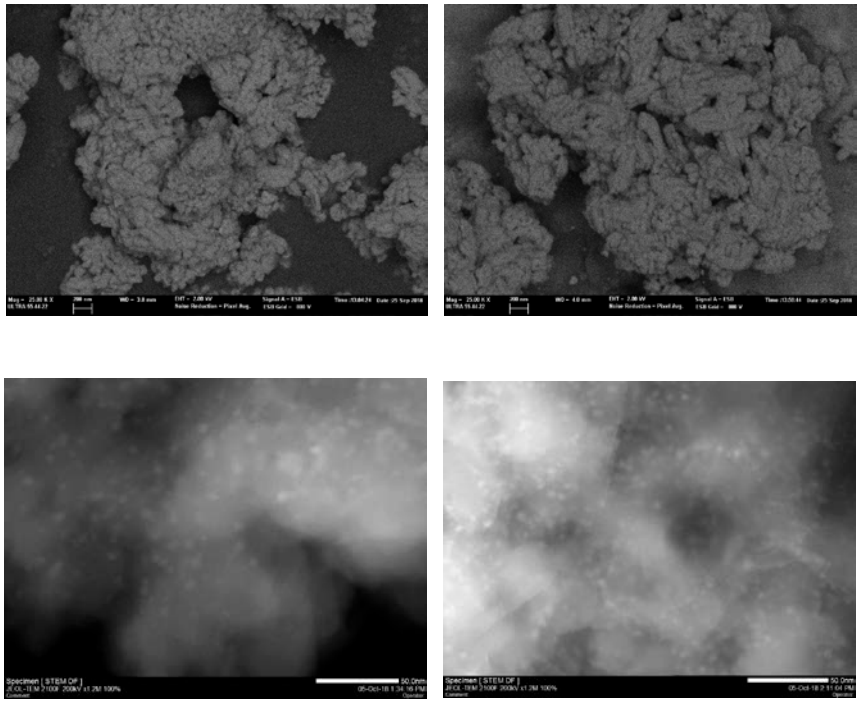

Fig. 2. FESEM (A) and STEM (B) images of Zn/ZSM-5 (left) and Zn-B/ZSM-5 (right)

The amount of boron added to the Zn/ZSM-5, 0.5 wt%, was selected based on previous works [14-16].

Figure 3 compares FESEM images taken with a secondary electron detector of the three zeolites. The images show that the three zeolites present comparable crystal size (<50 nm) and coffin-shaped morphology, forming larger aggregates, and that the Zn incorporation step does not alter the morphology of the ZSM-5 zeolites.

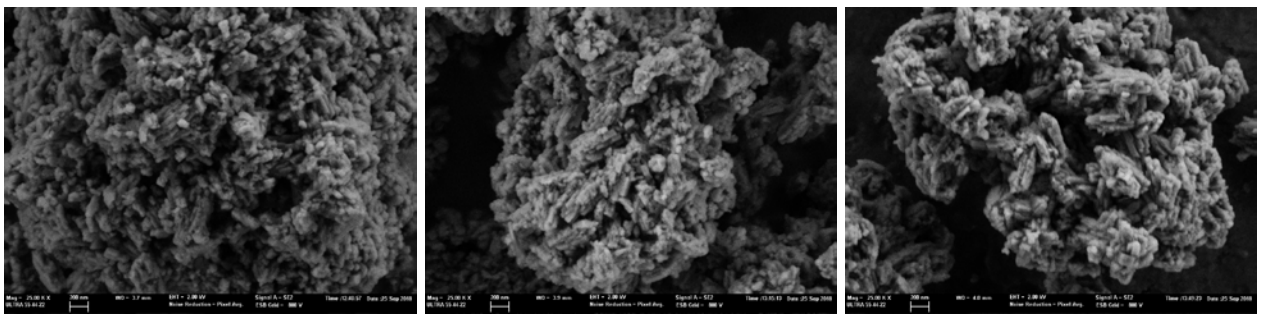

(A) (B) (C)

Fig. 3: FESEM images of ZSM-5 (A), Zn/ZSM-5 (B) and Zn-B/ZSM-5 (C)

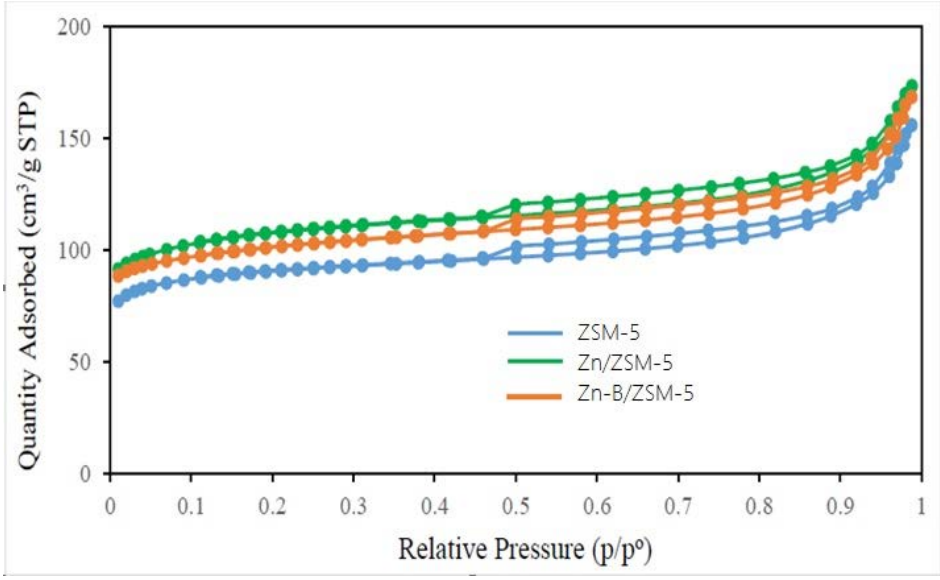

Fig. 4: N_2 adsorption−desorption isotherms of nano-ZSM-5 zeolite, Zn/ZSM-5 and Zn-B/ZSM-5.

Figure 4 provides the N_2 adsorption–desorption isotherms for ZSM-5, Zn/- and Zn-B/ZSM-5. The type I isotherms with a plateau at high relative pressures $p/p^0>0.9$ are those characteristic of microporous materials. Apparent hysteresis was observed in the relative pressure (p/p^0) range from 0.4 to 1.0 for all the samples, suggesting the presence of intercrystalline mesopores formed among smaller crystals [17, 18], as a consequence of their small size.

Table 1. Physico-chemical characteristics of the catalyst

Sample	Zn (%wt)	B (%wt)	S_{BET} (m^2/g)	S_{ext} (m^2/g)	S_{micro} (m^2/g)
ZSM-5	0	0	300	45	256
Zn/ZSM-5	5.3	0	359	53	306
Zn-B/ZSM-5	4.5	0.5	336	52	284

It is also observed that the Zn loaded ZSM-5 samples present a higher micropore surface area as compared to the Zn-free zeolite (see Table 1). This can be due to the removal of amorphous species present in the parent ZSM-5 during the Zn exchange step.

Mesopores' size distribution is shown in Fig. 5. The narrow peak centered at 4nm obtained for the three samples corresponds to the intercrystalline mesoporosity. Again, this agrees with the homogeneous and comparable crystal size of the three nano-crystalline zeolites, as observed by FESEM.

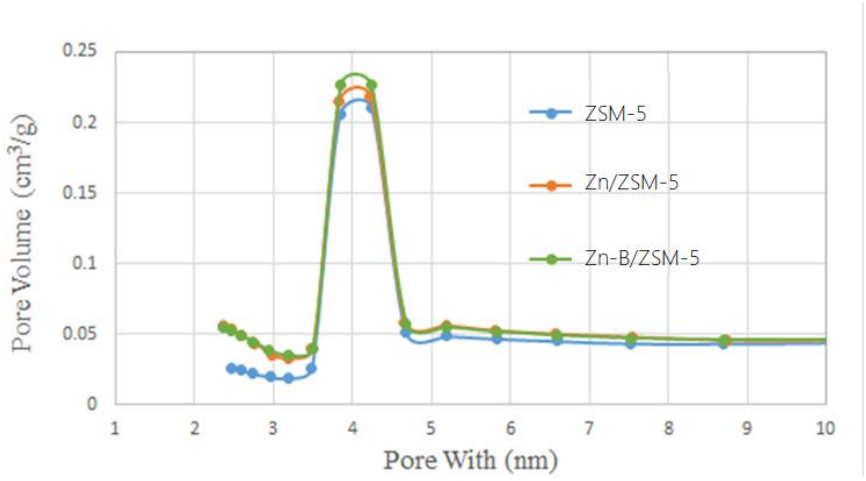

Fig. 5: Pore size distribution of nano-ZSM-5 zeolite, Zn/ZSM-5 and Zn-B/ZSM-5.

The three zeolites compared present the same Si/Al molar ratio of 13, as determined by ICP. In the case of the parent ZSM-5, the presence of this Al in framework positions of the zeolite compensated by protons, will result in Brønsted acidity.

The Py-FTIR spectra are shown in Fig 6. The band at ~1540 cm^{-1} corresponds to the interaction of the pyridine molecule with the Brønsted sites and those at ~1450 cm^{-1} are assigned to Lewis sites. The band at ~1490 cm^{-1} is attributed to both the Brønsted acid and Lewis acid sites [23]. To investigate the specific changes in the Brønsted and the Lewis

acidity of the catalysts, the ratio of the ~1540 and ~1450 cm^{-1} peak intensities (B/L ratio) was considered as a value to compare the relative amount of Brønsted and Lewis acid sites in the samples (see Table 2).

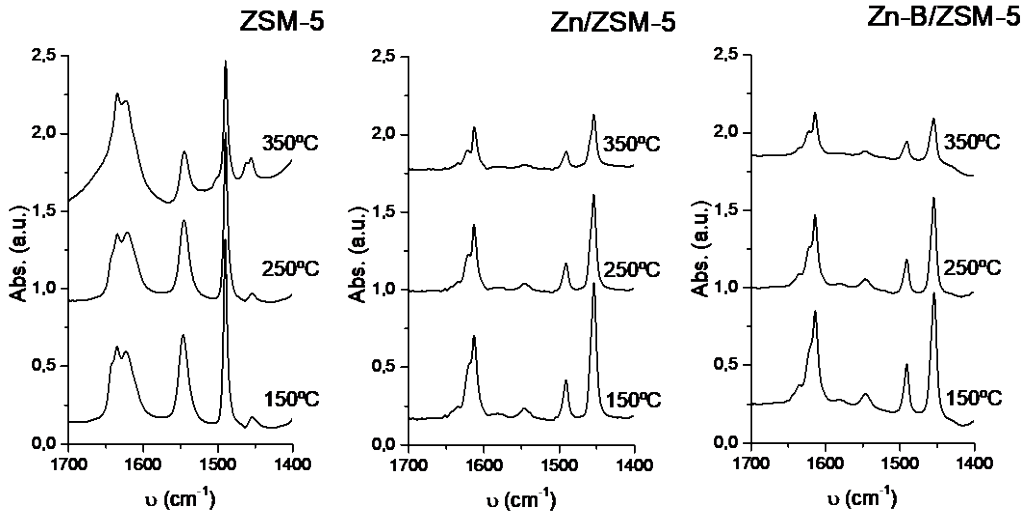

Fig. 6. Py-FTIR of nano-ZSM-5 zeolite, Zn/ZSM-5 and Zn-B/ZSM-5.

The reduction of the Brønsted acid site density and the high Lewis acidity indicate the presence of extra-framework cationic Zn species, occupying charge compensation positions instead of the original protons present in the Zn-free zeolite [12]. This would be in agreement with previous publications [23], where different extraframework Zn species were suggested such as [Al−O−Zn−O−Zn−O−Al] or [Al−O−Zn−O−Al], which acted as the Lewis acid sites. Moreover, the amount of framework Al is maintained as can be deduced from the comparable intensity of the peak at 55 ppm of the ^{27}Al MAS NMR (see Fig. 7). It can also be seen that after Zn addition the extraframework Al present in the parent ZSM-5 is eliminated as indicated by the disappearance of the band at 0 ppm assigned to aluminum in octahedral coordintation. This is an additional evidence for the removal of amorphous extraframework species present in the starting ZSM-5 during the Zn ion exchange step.

Table 2.Acidic properties of the catalyst

Sample	ZSM-5	Zn/ZSM-5	Zn-B/ZSM-5
Brønsted acidity (mmol Py/g)			
T=150ºC	0.690	0.079	0.107
T=250ºC	0.611	0.055	0.075
T=350ºC	0.386	0.024	0.039
Lewis acidity (mmol Py/g)			
T=150ºC	0.038	0.493	0.441
T=250ºC	0.030	0.371	0.356
T=350ºC	0.016	0.188	0.167
Lewis/Brønsted			
T=150ºC	0.06	6.24	4.12

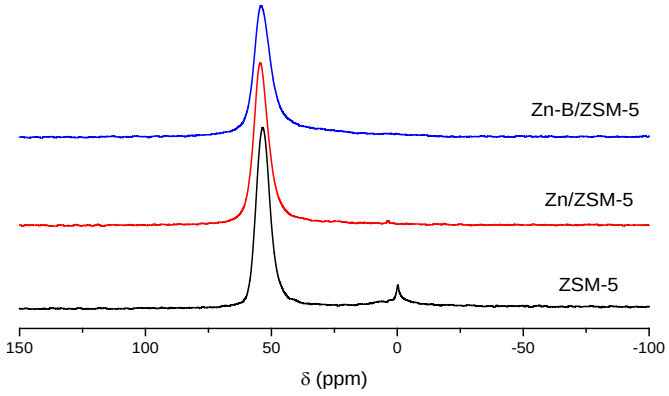

Fig. 7. ^{27}Al MAS NMR of nano-ZSM-5 zeolite, Zn/ZSM-5 and Zn-B/ZSM-5.

Regarding the addition of B, it does not significantly affect the acidic properties as can be deduced from Fig 6 and Table 2, although Brønsted acidity is slightly increased whereas the amount of Lewis sites is smaller than for the B-free Zn/ZSM-5. The lower Lewis acid site density and the increase in number of Brønsted acid sites can be related to the slight reduction in the Zn content, from 5.3 to 4.5 wt%.

^{11}B MAS NMR spectroscopy was used to study the coordination of the boron added, as this element is known to present a great degree of flexibility regarding its possible trigonal and tetrahedral coordination in boronsilicates [24]. It can easily be removed from zeolite framework positions under rather mild hydration conditions, but it can also reoccupy framework positions by dehydrations. The spectrum, shown in Fig. 8, presents two main bands, one centered at 13,7 ppm, assigned to non-framework trigonal B species, with no B-O-Si links, such as $B(OH)_3$, and one band at 0.3 ppm, assigned to trigonal framework boron species, $(B(OSi-)_2OH$, generating defect sites. This latter band has a shoulder at lower chemical shifts (-3.2 ppm) assigned to tetrahedral framework B species formed by hydration, $B(OSi-)_2(OH)_2$ [24]. Thus, at least part of the added B is occupying framework positions, leading to Brønsted sites of reduced acidity [25, 26].

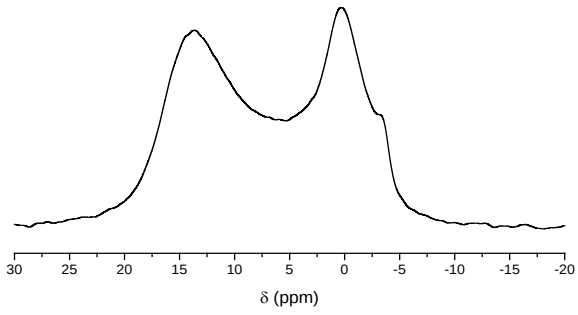

Fig. 8. ^{11}B MAS NMR of Zn-B/ZSM-5

3.2. Catalytic performance.

A first set of experiments was performed in order to determine the optimum temperature for the aromatization of n-hexane catalyzed by the Zn/ZSM-5 samples, and the results obtained for conversion of the alkane and selectivity to aromatics are shown in Fig. 9.

When the temperature is increased in the range of 350ºC to 550ºC, the n-hexane conversion obtained after 5 hours on stream increases significantly. Selectivity to aromatics is also increased when temperature is increased from 350 to 500ºC. Thus, high reaction temperatures favor the aromatization reaction in good agreement with previous works, where detailed product analysis show that light olefins are the main products at low temperatures and/or low conversions, and that higher alkane conversion and high concentration of olefin precursors in the reaction media are needed for production of aromatics [27-29]. As zinc may volatilize at high temperature [1] and the improvement in conversion and selectivity when going from 500ºC to 550ºC was not too big, 500ºC was the temperature chosen for comparing the B-free and the Zn-B/ZSM-5 samples as catalysts for the aromatization reaction.

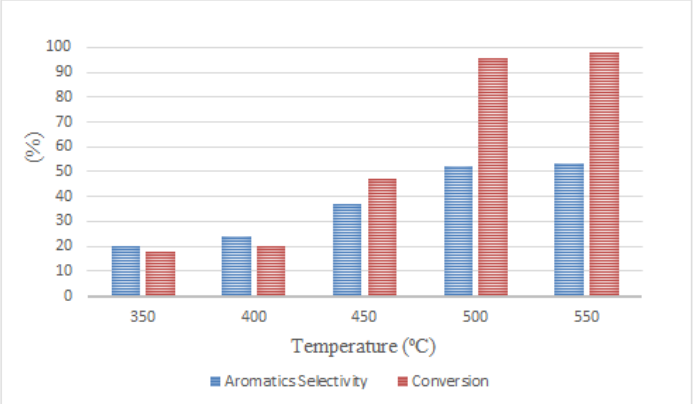

Fig. 9. Influence of temperature on the catalytic behavior of Zn/ZSM-5

The catalytic conversion of n-hexane obtained in the presence of Zn/- and Zn-B/ZSM-5 catalyst under the same experimental conditions is given in Fig. 10.

The initial n-hexane conversion on Zn/ZSM-5 (95%) was higher than that on Zn-B/ZSM-5 (~92%). The selectivity to aromatics is in the range of previous papers working under similar conditions, and light olefins, mainly propylene and butenes, are expected to complete the product distribution [1]. At this point we have to consider the bifunctional reaction mechanism described for the alkane aromatization on Zn/ZSM-5 catalysts. First, the alkane, in this case n-hexane, has to be dehydrogenated on the Lewis acid sites, associated to dispersed cationic Zn species. According to the acidity measurements presented in Table 2, the total amount of Lewis acid sites decreases after incorporation of B, so this would justify the slightly lower initial activity of Zn-B/ZSM-5. However, for longer times on stream a larger decrease in the conversion of n-hexane was observed on Zn/ZSM-5 as compared to the B-containing catalyst, which was attributed to catalyst deactivation due to coke formation [1]. Thus, the presence of boron retards the deactivation of the catalyst as shown in Fig. 10. Here, we have to consider the reaction mechanism again, as in a second step, the olefin produced by dehydrogenation on the Zn species will oligomerize and/or ciclate on the Brønsted acid sites. Incorporation of boron in framework positions, as shown by the ^{11}B-MAS NMR results, is known to influence the acidic properties of the final catalyst, reducing the acid strength of the Brønsted sites [25, 26]. Thus, the insaturated intermediates will be adsorbed more weakly on these sites, the residence time of these coke precursons on the acid sites will be lower and deactivation rate by coking will be reduced as described for other proceses [26]. This is, indeed, what we observe (see Fig.10).

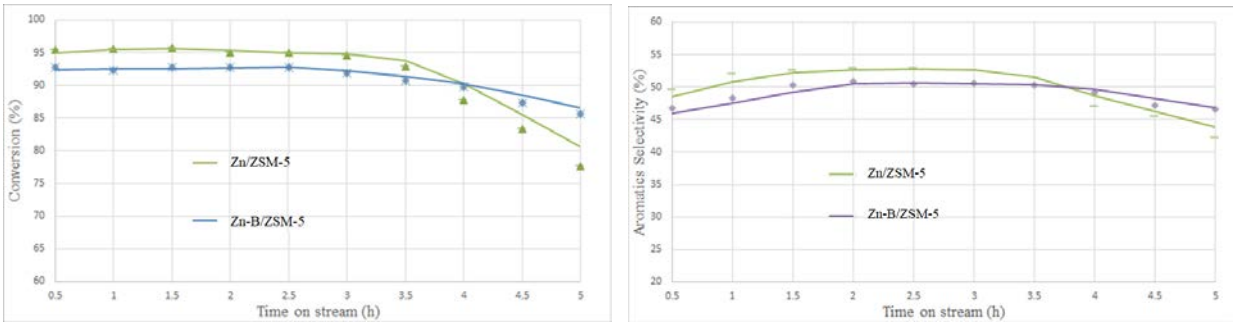

Fig. 10. n-Hexane conversion and selectivity to aromatics of Zn/ZSM-5 and Zn-B/ZSM-5 with time-on-stream obtained at 500ºC.

Conclusions

Zn/ZSM-5 and Zn-B/ZSM-5 catalysts were prepared and tested as catalysts for aromatization of n-hexane. Introducing Zn onto the ZSM-5 zeolite did not affect the ZSM-5 structure and, according to the Py-FTIR results, the incorporation of zinc results in an important increase of the Lewis acid site density of the catalysts, and in a reduction of the Brønsted acid sites. Thus, cationic Zn species, highly dispersed, will be located at ion exchange positions, substituting the protons present in the parent ZSM-5. The addition of boron recovers some Brønsted acidity, and at least part of it is occupying framework positions, leading to Brønsted sites of reduced acidity. Boron incorporation has a clear effect on the catalytic behaviour of the Zn/ZSM-5 catalysts, with the boron-free sample being more active initially, but deactivating at a higher rate with time on stream than the boron promoted catalyst.

Acknowledgements

This research is funded by Vietnam National Foundation for Science and Technology Development (NAFOSTED) under grant number 104.05-2018.306, by the Spanish Government-MICINN through ‘Severo Ochoa” (SEV-2016-0683) and RTI2018-101033-B-

I00, by the Fundación Ramón Areces through a research contract of the “Life and Materials Science” program, and by Generalitat Valenciana through AICO/2019/060. The Electron Microscopy Service of the UPV is acknowledged for their help in sample characterization. We thank E. Briz for technical assistance.

References

1. T.E. Tshabalala, M.S. Scurrell, Catalysis Communications, 72 (2015) 49–52.

2. V. Fila, M. Bernauer, B. Bernauer, Z. Sobalik, Catalysis Today, 256 (2015) 269–275

3. J.A. Johnson, J.A. Weiszmann, G.K. Hilder and A.H.P. Hall, Paper presented at the 1984 NPRA Annual Meeting, March 25-27, 1984, San Antonio, Texas.

4. D. Bhattacharya, S. Sivasanker, Appl. Catal. A, 141 (1996) 105-115.

5. N.Y. Chen and T.Y. Yah, Ind. Eng. Chem. Process. Des. Dev., 25 (1986) 151.

6. M. Guisnet, N.S. Gnep, F.Alario, Appl. Catal. A, 89 (1992) 1-30.

7. Y. Ono, Catalysis Reviews: Science and Engineering, 34:3 (1992) 179-226;

8. P. Mériaudeau, C. Naccache, Catalysis Reviews, 39:1-2 (1997) 5-48;

9. S. R. Kanitkar, J. J. Spivey, Natural Gas Processing from Midstream to Downstream, Chapter 14 (N. Elbashir, M.M. El-Halwagi, I.G. Economou, K.R. Hall, Eds.), 2019, John Wiley & Sons Ltd.

10. N. Viswanadham, A.R. Pradhan, N. Ray, S.C. Vishnoi, U. Shankar, T.S.R. Prasada Rao, Appl. Catal. A 137 (1996) 225

11. E. Rojasova, A. Smieskova, P. Hudec, Z. Zidek, Collect. Czech. Chem. Commun. 64 (1999) 168-176.

12. S. M. T. Almutairi, B. Mezari, P. C. M. M. Magusin, E. A. Pidko, E. J. M. Hensen, ACS Catal. 2 (2012) 71-83.

13. X. Niu , J. Gao. Q. Miao, M. Dong, G. Wang, W. Fan, ,Z. Qin, J. Wang. Microporous and Mesoporous Materials 197 (2014) 252–261.

14. J. Xu and M. Saeys, J. Catal. 242 (2006) 217-226

15. Q.T. Trinh, T.H. Pham et al, Catal. Sci. Technol. 6 (2016) 5871 - 5883.

16. J.B. Kimble, C.A. Drake, J. Yao, A. Hu (Phillips Petroleum Co), US patent US6156689A, 1997

17. G.-l. Wang, W. Wu, W. Zan, X.-f. Bai, W.-j. Wang, X. Qi, O.V. Kikhtyanin, Trans. Nonferrous Met. Soc. China, 25 (2015) 1580−1586.

18. Y. Ni, A. Sun, X. Wu, G. Hai, J. Hu, T. Li, G. Li, Microporous and Mesoporous Materials 2011 (143) 435−442.

19. F. Yaripour, Z. Shariatinia, S. Sahebdelfar, A. Irandoukht, Microporous and Mesoporous Materials 203 (2015) 41-53.

20. IZA Database of Zeolite Structures, The pentasil Family (http://europe.iza-structure.org/IZA-SC/intergrowth_families/Pentasils.pdf);

21. G. Perego, M. Cesari, G. Allegra, J. Appl. Cryst. 17, (1984) 403-410;

22. G. Perego, G. Bellussi, A.Carati, R. Millini, V. Fattore, ACS Symp. Series 398, (1989) 360-373.

23. P.T. Huyen**,** L.T.H. Nam, T.Q. Vinh, C. Martinez, V.I. Parvulescu, Catalysis Today 306 (2018) 121-127

24. S.-J. Hwang, C.-Y. Chen, S. I. Zones, J. Phys. Chem. B, 2004, 108, 18535-18546.

25. M.G.Howden, ZEOLITES 1985, Vol 5, 334-338.

26. F. Yaripour, Z. Shariatinia, S. Sahebdelfar, A. Irandoukht, Microporous and Mesoporous Materials 203 (2015) 41-53.

27. D.K. Simmons, R. Szostak, P.K. Agrawal, T.L. Thomas, J. Catal 106 (1987) 287-291.

28. J. Kanai, N. Kawata, J. Catal. 114 (1988) 284-290.

29. A. Smiešková, E. Rojasová, P. Hudec, L. Šabo, React. Kinet. Catal. Letters 82, 2004, 227-234.